

# Influence of media disorder on DNA melting

Debjyoti Majumdar<sup>1,\*</sup>

<sup>1</sup>*Alexandre Yersin Department of Solar Energy and Environmental Physics, Jacob Blaustein Institutes for Desert Research, Ben-Gurion University of the Negev, Sede Boqer Campus 84990, Israel*

(Dated: September 18, 2024)

Motivated by the fractal form of the compact chromatin in vivo, we study the melting of a lattice DNA on the infinite cluster backbone near the three-dimensional site percolation critical point ( $p_c = 0.3116$ ), which exhibits fractal-like properties, using Monte Carlo simulations. Further, we extend our study to other values of atmospheric disorder ( $p_c \leq p \leq 1$ ) and show how the melting temperature varies with a decrease in the availability of lattice sites mimicking the crowded environment inside the cell nucleus. Importantly, we found that the melting transition sharpens with a linear increase in the denaturation temperature as we increase the degree of disorder. Two separate disorder regimes showing weak and strong effects on melting can be identified. For simulations, we use the pruned and enriched Rosenbluth method in conjunction with a depth-first implementation of the Leath algorithm to generate the underlying disorder.

## I. INTRODUCTION

Understanding the influence of disorder on the critical behavior of physical systems is one of the crucial problems in statistical and condensed matter physics. Broadly, disorder implies the presence of elements that alter the behavior of the pure system, e.g., non-magnetic impurities in magnetic systems that can modify the magnetic response [3]. For systems showing critical phenomena, the possibility of a new universality class arises when the specific heat exponent  $\alpha > 0$  – known as the Harris criterion [19].

For biological systems like DNA, the intracellular components such as proteins, lipids, saccharides, etc. – collectively called “macromolecular crowders” – play the role of atmospheric [1] disorder [14, 31, 34, 41, 43]. These biomolecules occupies about 20-40% of the volume and, thereby, can potentially modify DNA functionality by restricting the spatial volume available to the DNA. Few theoretical and experimental studies performed in this direction have shown that the melting temperature linearly increases with the density of crowders [10, 20, 23, 24, 39] and renaturation rate increases by 1-2 orders of magnitude under crowded conditions [38, 47], while in some cases a decrease in the melting temperature was observed too [35]. Crowding is also associated with multiple other biological functionalities [50]. However, it is still unclear how the degree of disorder affects the nature of the melting transition.

For systems defined on the lattice, the usual way to realize a disordered background is to use percolation-type models where sites diluted with a certain probability are rendered non-functional or differently functional than their typical behavior in the non-diluted system. Whereas a large number of studies in the last few decades has been devoted towards understanding the changes in the polymer scaling laws in disordered lattices

[5, 25, 32, 37, 40], studies concerning disorder-induced changes in DNA melting using lattice-based models, remains less explored. Of particular importance is the question of whether a melting transition exists at all in the limit where the density of available sites is close to the percolation threshold and the underlying lattice is a fractal characterized by a few broken dimensions [44]. The additional diverging length scale at the percolation critical point is expected to make things complicated, which demands further attention and careful study using simplistic but versatile DNA models, which can be easily integrated with models of percolation and allow usage of powerful numerical techniques at the same time.

Additionally, melting on the fractal infinite cluster at the percolation threshold has some special relevance per se since the chromatin in its compact form exhibits fractal-like properties, with a fractal dimension  $d_f = 2.4 (< 3)$  as revealed from small angle neutron scattering experiments [33]. This fractal form gives rise to anomalous properties, e.g., sub-diffusive dynamics of chromosomal loci [45], not only with active forces in a non-equilibrium backdrop but also for the thermal equilibrium scenario [30, 42, 46]. Although the scenarios concerning the fractal form of chromatin and melting on a fractal lattice are seemingly different, it is plausible that the underlying fractal structure preserves some universal features that would be reflected in both situations.

In this paper, therefore, we present results for simulations of DNA melting on the infinite cluster backbone at the site percolation threshold ( $p_c = 0.3116$ ) of the three-dimensional cubic lattice and also for other values of disorder ( $p \geq p_c$ ), using a lattice adaptation of the Poland-Scheraga model [8, 36] for the DNA. The phase diagram demonstrating how the melting temperature varies with the degree of disorder is mapped out, and the changes in the associated scaling exponents and order parameter distribution at the transition points are investigated. Further, we also study the bubble formation statistics, which is believed to be related to crucial functionalities of the DNA, from providing flexible hinges to fold [15, 49] to initiation of transcription [12]. Below  $p_c$ , the clusters are

\* debjyoti@post.bgu.ac.il

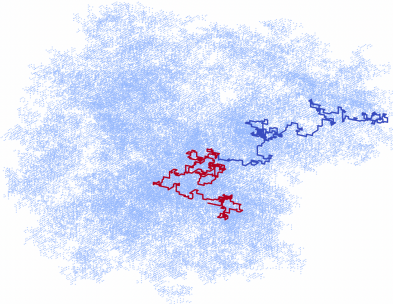


FIG. 1. An unbound DNA configuration of length  $N = 400$  grown over a disordered lattice with site existence probability  $p = 0.312$ . The cloudy background represents the disordered lattice with white patches representing diluted sites created out of a cubic lattice of side  $L = 499$ .

disconnected such that they cannot support a chain of infinite length (thermodynamic limit), and, therefore, the question of a phase transition is moot. Other than the melting transition, we report possible enhancements in the numerical algorithm, which could enhance the sampling of polymers in disordered media, and has not been reported before, to the best of our knowledge.

The rest of the paper is organized in the following manner: in Sec. II, we introduce the models for DNA and lattice disorder. Sec. III discusses the simulation techniques for introducing lattice heterogeneity and growing the DNA strands on it. In Sec. IV, the observables of interest, the associated scaling forms, and the method of disorder averaging are discussed. In Sec. V, we discuss the findings on how a disordered environment modifies the DNA melting transition with particular emphasis on melting near the infinite percolating cluster, and finally conclude our paper in Sec. VI.

## II. OUR MODEL FOR DNA AND DISORDER

We use the DNA model introduced in Ref. [8] and later used in studying multiple scenarios of DNA melting [26–29]. This model is a lattice adaptation of the famous Poland-Scheraga (PS) model [36]. The model considers two distinct self-avoiding walks ( $\mathbf{r}_i^A, \mathbf{r}_j^B$ ) originating from the center of a cubic lattice representing the double strands of the DNA. The strands obey self-avoidance both with monomers from their own and with that of the other strand. The only exception is for monomers with the same position index along the strands, which can occupy the same lattice site ( $\mathbf{r}_i^A = \mathbf{r}_i^B$ ) resulting in an energetic gain of  $-\epsilon$ , thereby, mimicking the hydrogen-base pairing in DNA. With every base pairing, we associate a Boltzmann factor  $q = \exp(\epsilon/k_B T)$ , where  $T$  is the temperature and the Boltzmann constant  $k_B$  is set to 1 throughout our simulations. The Hamiltonian describing a typical configuration would be

$$\mathcal{H} = -\epsilon \sum_{i=1}^N \delta_{\mathbf{r}_i^A, \mathbf{r}_i^B}, \quad (1)$$

where  $\delta_{i,j}$  is the Kronecker delta counting the number of base-pair contacts. From here onwards, we will refer to the maximum number of possible base pairs ( $N$ ) as the DNA's length.

To model the background disorder, we randomly dilute sites across the cubic lattice [see Fig. 1]. Diluted sites are then no longer available to grow the DNA chain/s. The defects generated this way are spatially uncorrelated. This underlying lattice inhomogeneity, in a way, serves as a model for crowders *in vivo*, with the density of diluted sites corresponding to the crowder density. However, modeling this way, we assume crowders of uniform sizes only, which are frozen in time or with a relaxation time much larger than the time the DNA would take to sample different regions of the available volume within the observation time.

Our model, therefore, simplifies the actual complex situation by coarse-graining microscopic details at different levels, e.g., we neglect the sequence heterogeneity along the DNA strands, the difference in bending rigidity among the bound and unbound segments, helical topology, polydispersity of the crowders, etc. While our model cannot explicitly include some of these features, e.g., helicity, including others would only make the problem infeasible to study along with a disordered background. Therefore, we plan to consider some of these separately in future works.

## III. SIMULATION TECHNIQUES

### A. Lattice disorder generation method

We use the Leath algorithm to generate the infinite cluster at the site percolation threshold ( $p_c$ ) and also for other disorder values  $p > p_c$ . Starting from the center of a cubic box, which we assume to be occupied, and later serve as the starting point of the DNA configurations, the neighboring sites are visited and occupied with probability  $p$ . If chosen unoccupied, we still mark the site as visited so that it will not be considered for occupancy in the future to ensure random but uniform dilution of sites. If the recent site is occupied, we further perform a recursive depth-first search and occupy for the neighbors of the current site. This continues as long as the pointer does not try to step out of the simulation box or there are no more available unvisited neighboring sites. Once stuck, the pointer returns to the last occupied site and continues with its other neighbors. To ensure that an infinite cluster exists ( $p = p_c$ ), we check if the cluster being generated touches all six faces of the cube. If the cluster fails to connect all six faces, we discard the current realization and start with a new one.

To avoid boundary effects of the finite simulation box containing the disordered lattice, we used lattices of linear dimension  $L = 599$ , much larger than that would be required by SAWs even at  $p_c$  with a modified size exponent  $\nu_{\text{SAW}}(p_c) = 0.667$  [5]. To ensure the fractality of the infinite cluster at the percolation threshold, we calculate the mass fractal dimension ( $d_f$ ) given by the scaling of the number of sites with the radius ( $r$ ) of concentric circles,  $M \sim r^{d_f}$ , with the center chosen at the cluster's center of mass. For three-dimensional site percolation, the value is precisely known to be  $d_f = 2.52$  [44], which matches well with our estimate.

## B. Polymer generation method

To simulate the DNA strands on the diluted lattice obtained using the method mentioned in Sec. III(A), we use the pruned and enriched Rosenbluth method (PERM) [2, 17]. Two strands of the DNA are grown simultaneously while monomers are added to the last monomer of both strands at once. At each step, we calculate the combined possibilities of free sites to step obtained by a Cartesian product of the individual sets of free sites for each strand, i.e.,  $\mathcal{S}_n = \mathcal{S}_n^A \times \mathcal{S}_n^B$ , where  $\mathcal{S}_n^A$  and  $\mathcal{S}_n^B$  are the individual sets of possible free sites. Each element in  $\mathcal{S}_n$  represents an ordered pair of new steps for both the strands and importance given by the Boltzmann weight  $q = \exp(\epsilon\beta)$  for a base-pair contact and 1 otherwise. The choice is made by picking a uniform random number  $\in [0, w_n]$ , where  $w_n = \sum_{\mathcal{S}} \exp(\beta\epsilon\delta_{r_i^A, r_i^B})$  is the local partition sum, and then finding the  $\mathcal{S}_n$  element it corresponds to. The partition sum at length  $n$  for the current tour is calculated by product over the local partition sums at each step,  $W_n = \prod_{i=1}^n w_i$ . Averaging  $W_n$  over the number of started tours then gives the average partition sum,  $Z_n = \langle W_n \rangle$ .

Enrichment and pruning at  $n$ th step is performed depending on the ratio,  $r = W_n/Z_n$  and using the scheme:

$$r = \begin{cases} < 0.9, & \text{prune with probability } (1 - r) \\ [0.9, 1.1], & \text{continue to grow} \\ > 1.1, & \text{make } k\text{-copies.} \end{cases} \quad (2)$$

If  $r < 0.9$  and pruning fails, the configuration is continued to grow but with  $W_n = Z_n$ . For enrichment ( $r > 1.1$ )  $k$  is chosen as,  $k = \min(\lfloor r \rfloor, \mathcal{N}(\mathcal{S}_n))$ , where  $\mathcal{N}(\mathcal{S}_n)$  is the cardinality of the set  $\mathcal{S}_n$ , and each copy is continued with a weight  $\frac{W_n}{k}$ .

For estimating thermodynamic observable  $Q_n$  at length  $n$ , the averaging is performed on the fly using the expression:

$$\langle Q_n \rangle(q) = \frac{\langle Q_n W_n(q) \rangle}{Z_n(q)}, \quad (3)$$

where the  $\langle \dots \rangle$  in the numerator represents the running average of the quantity over number of started tours, using the local estimate of the configuration weight  $W_n(q)$ .

## C. Additional bias

One of the popular ways to avoid polymer growth from getting stuck in constrained geometries, e.g. on cylinder, is to use *Markovian anticipation* [13] where depending upon  $k$ -steps statistics at length  $m$ , we decide what should be the choice for the future step at length  $n$  depending upon the sequence of  $(n-k-1) \dots (n-1)$  steps. However, when we try to apply this bias for growth in a disordered lattice, we must prepare the initial set  $k$ -step statistics for each disorder realization. Hence, we need a scheme that can bias only depending on the local density of diluted and occupied sites. Thus, in addition to associating weights to base-pair contacts, to favor the growth of chains towards a less diluted zone, we apply an extra directional bias in which the next steps of the walkers are biased in the direction of the pyramidal cone formed by the  $h$  successive layers in front of the strand's growth end corresponding to each  $s_n \in \mathcal{S}_n$ , which has the lowest diluted and occupied sites. The weight used for such a bias is of the form  $f_{bias} = \frac{n_{as}}{(n_{os}+1)}$ , where  $n_{as}$  and  $n_{os}$  are the number of total available sites and the number of occupied sites within the volume of the pyramid, respectively, for each  $s_n \in \mathcal{S}_n$ . Note, that the 1 in the denominator avoids divergence if  $n_{os} = 0$ . The depth of the pyramid determines how far the walker sees before taking the next step. The dimensions of the scanning pyramid are determined by the height  $h$ , and the base, which is a square of width  $2h$ . The time required to scan the pyramidal volume increases like  $\mathcal{O}(h^3)$ . In our simulations, we use  $h = 3$ . With the introduction of this extra bias, the expression for calculation of weights at each step has to be modified as  $w_n = \sum_{j \in \mathcal{S}} \exp(\beta\epsilon\delta_{r_i^A, r_i^B}) f_{bias}^j$ . Of course, at each biased step, the inclusion of the local weights needs to be corrected by the biasing factor for the corresponding direction of the chosen steps, i.e.,  $W_n/f_{bias}^j$ , where  $f_{bias}^j$  is the biasing factor for that particular direction.

## IV. OBSERVABLES SCALING AND AVERAGING

To study the DNA strand separation transition we look at the average number of bound base-pairs ( $n_c$ ) at different temperatures which serves as the order parameter. Under a change of temperature or equivalently of the Boltzmann factor from  $q = \infty$  to  $q = 0$ ,  $n_c$  goes from  $n_c/N = 1$  (bound) to 0 (unbound) phase. At the transition point we have the following scaling  $n_c \sim N^\phi$  where the exponent  $\phi$  controls the sharpness of the transition. For first-order transition  $\phi = 1$ , and  $\phi = 1/2$  for continuous transition with the excluded volume interaction switched off (for ideal chains) [8]. The thermal response is obtained from the fluctuation of  $n_c$  and is given by  $C_c = \langle n_c^2 \rangle - \langle n_c \rangle^2$ , where the  $\langle \dots \rangle$  denotes averaging over configurations. The quantity  $C_c$  follows the scaling form  $C_c \sim N^{2\phi} g[(q - q_m)N^\phi]$  near the transition point.

Therefore, we will get data collapse on plotting  $C_c/N^{2\phi}$  vs.  $(q - q_m)N^\phi$  using which we will extract the melting points  $q_m$  and exponent  $\phi$ .

Further, we find the bubble size distribution  $P(\ell_b)$  at the transition points, where it has been shown to follow a power law distribution of the form  $P(\ell_b) \sim \ell_b^{-c}$ , where  $c$  is called the bubble-size or reunion exponent. For first-order transition  $c \geq 2$ , and  $1 < c < 2$  for continuous transition. Further for continuous transition we have  $\phi = c - 1$  [7]. The effect of disorder on the average number of bubbles ( $n_b$ ), and the average bubble length ( $\ell_b$ ) is also studied. We define the size of a bubble ( $\ell_b$ ) as the number of contiguous broken bonds enclosed within two bound segments. Note that, due to the discrete nature of the lattice the minimum size of a bubble starts from  $\ell_b = 2$ .

We also looked at the base-pair contact probability distribution ( $P_{n_c}(q_m)$ ) at different lengths close to the transition points. To calculate  $P_{n_c}(q)$  we use the following formula

$$P_{n,n_c}(q) = \frac{Z_{n,n_c}(q)}{\sum_{n_c=0}^n Z_{n,n_c}(q)}, \quad (4)$$

where  $Z_{n,n_c}(q)$  is the constrained partition sum at length  $n$  with the number of base-pair contacts  $n_c$ . For the DNA model in hand the probability distribution is expected to follow the scaling form  $P_{n_c,N} \sim N^{-\phi} p(n_c/N^\phi)$  [8].

While averaging over different disorder realizations, the convergence of results can be sensitive to the number of independent disorder realizations ( $\eta_1$ ), and the number of independent samples (here called ‘‘tours’’) ( $\eta_2$ ) used for averaging over each disorder realization. They will be characterized by two different variances: ( $\sigma_1$ ) and ( $\sigma_2$ ). Keeping  $\eta_2$  large would give PERM sufficient time (in terms of the number of tours) to explore one single disordered lattice configuration (initially). Since, on average, the number of available sites in concentric circles should scale similarly (for a given  $p$ ), it would not be difficult for PERM to calibrate the average weights from the next realization onwards. On the other hand, too large  $\eta_2$  values would reduce the diversity in disorder realizations when simulations run for a finite time. For our purpose, we found  $\eta_2 = 10^4$ , and  $\eta_1 = 10^9$  to give sensible results. However, on-the-fly schemes can be devised where  $\eta_2$  is calibrated for each new disorder configuration depending upon  $\sigma_2/\sigma_1$  [3].

Besides the averaging performed over multiple tours (thermal fluctuations) for a given instance of disorder – denoted by  $\langle \dots \rangle$  – we also need to perform averaging over distinct disorder realizations which we denote by  $[\dots]$ . Doing so, we notice that the disorder averaging of an observable  $[\langle Q_n \rangle]$  can be done at two different levels; first, the average can be taken over  $\langle Z_n \rangle$  which would give us the annealed free energy  $f_a = -\beta^{-1} \ln [Z_N]$  and the expression for evaluating a disorder averaged observable will then be given by,

$$[\langle Q_n \rangle]_a = \frac{[\langle Q_n W_n \rangle]}{[\langle Z_n \rangle]}. \quad (5)$$

In the second kind of average, the disorder averaging is taken over the logarithm of  $Z_n$  as  $[\ln \langle Z_n \rangle]$  which gives the quenched free energy  $f_q = -\beta^{-1} [\ln Z_N]$ . Here, an averaged observable  $[\langle Q_n \rangle]$  will be given by,

$$[\langle Q_n \rangle]_q = \left[ \frac{\langle Q_n W_n \rangle}{\langle Z_n \rangle} \right] = \frac{1}{C} \sum_C \frac{\langle Q_n W_n \rangle}{\langle Z_n \rangle}, \quad (6)$$

where  $C$  is the number of independent disorder configurations generated which has at least one DNA sample of length  $n$  for the  $\langle \dots \rangle$  average. The way PERM is implemented, it is perhaps easier to implement Eq. (5). Again, since one of the ends of our model DNA remains pinned at the origin, one can argue, our study corresponds to the ‘‘quenched’’ problem [11].

## V. RESULTS AND DISCUSSION

*Regular lattice:* The unbinding phase transition of a duplex DNA is the result of an underlying mechanism trying to minimize the free energy density by increasing the entropy of the system according to the equation  $F = U - TS$ , where  $U$  and  $S$  is the energy density and entropy per unit length, respectively, at a constant temperature  $T$ . For the model considered here, the melting point on a regular lattice, i.e.,  $p = 1$ , is  $q_m = 3.825$  [8] and the melting transition was discontinuous (first-order), with an exponent value  $\phi \approx 1$  [8]. Across a first-order melting point  $F_{q \rightarrow q_{m-}} = F_{q \rightarrow q_{m+}}$ , therefore, change in  $F$ ,  $\Delta F|_{q=q_m} = 0$  yielding  $T_m = \frac{\Delta U}{\Delta S}$ . One can identify the bound phase as the energy-dominated state and the unbound phase as the entropy-dominated state, with the melting temperature ( $T_m \equiv q_m$ ) determined by an interplay between  $\Delta U$  and  $\Delta S$ . Note that while  $\Delta U = 1$  is fixed while going from bound to unbound phase,  $\Delta S$  usually depends on the connectivity of the underlying lattice, which will play an important role in the present study.

*Phase diagram:* In Fig. 2, we show the phase diagram of melting ( $q_m$ ) as a function of lattice disorder ( $p$ ), where  $1 - p$  is the probability with which a site is diluted. On introducing lattice disorder (i.e.,  $p < 1$ ), we found that the melting temperature increases (or equivalently  $q_m$  decreases) linearly with  $p$ . The melting points ( $q_m$ ) are estimated from data collapse of the order parameter [see Fig. 2(a)] and its fluctuation [Fig. 2(b) and (c)] at different lengths across the melting transition, extracting the exponent  $\phi$  at the same time. The linear increase in  $T_m$  was also observed both in theoretical [39] and experimental [16] studies. The increase in the melting temperature is a result of the fact that while entropy ( $S$ ) goes down when sites are increasingly less available, and  $|\Delta U| = 1$

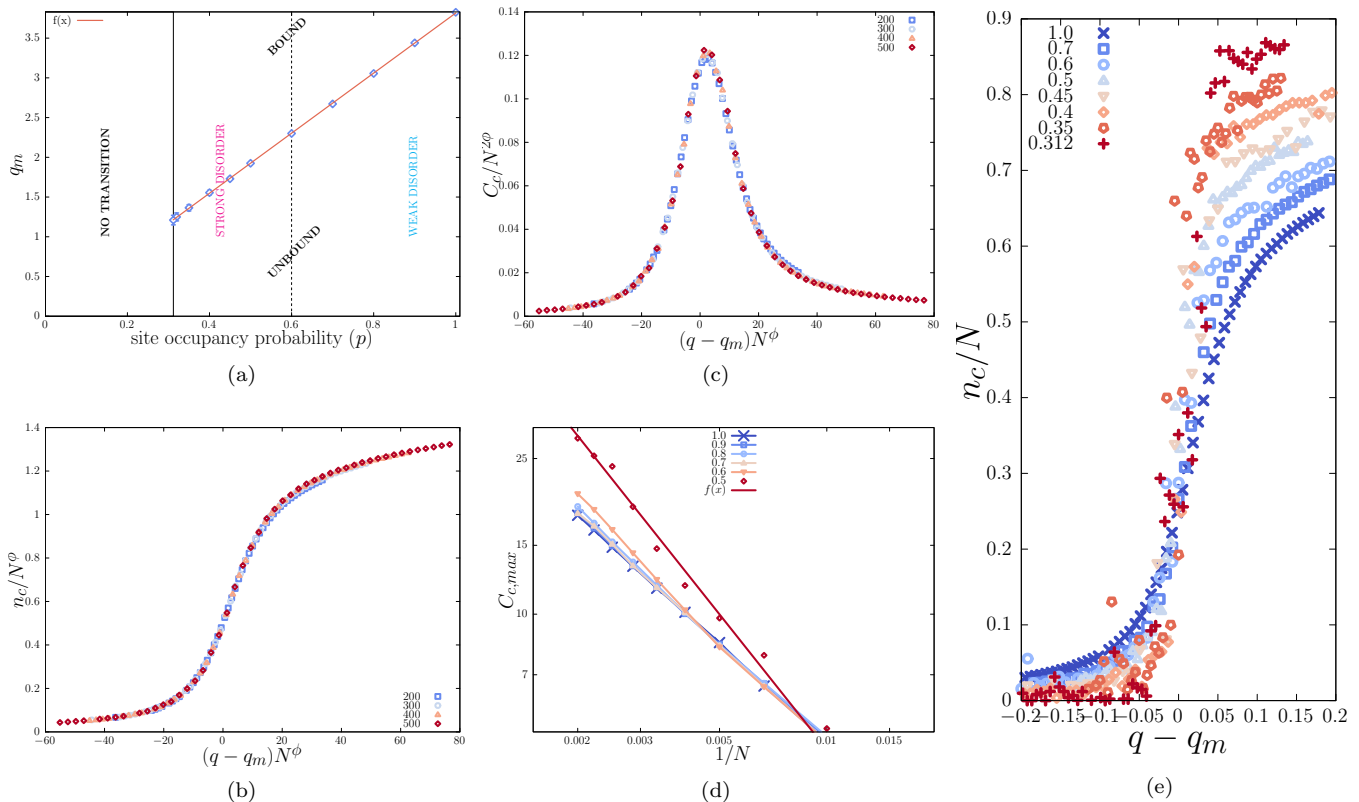


FIG. 2. **Melting vs. disorder phase diagram, order parameter and its fluctuation scaling** (a) We plot the Boltzmann factor for forming a base pair at the melting point ( $q_m$ ) along the y-axis and the site occupancy probability ( $p$ ) along the x-axis. The line  $f(x)$  is a straight line fit of the data points (diamonds) with estimated slope  $m = 3.78196 \pm 0.01048$  and y-intercept  $c = 0.0354181 \pm 0.006505$ . The error bars in  $q_m$  along the y-axis are of the sizes of the plotting points and increase towards  $p_c$ . The region “NO TRANSITION” refers to  $p < p_c$  and consists of disconnected clusters with no possible phase transition. The dashed vertical line at  $p = 0.6$  separates the regions of strong and weak influence of disorder on melting. (b) Scaling plot of average number of base-pairs in contact across the melting transition for  $p = 0.8$  using  $\phi = 0.9$  and  $q_m = 3.055$ . (c) Data-collapse of  $C_c$  data for  $p = 0.8$  as shown in (b), using the same  $q_m$  and  $\phi$  as in (b). (d)  $C_c$  peaks for different  $p$  values vs. system size inverse ( $N^{-1}$ ).  $f(x) \sim N^{-b}$  is a fit of the of the  $p = 0.5$  datapoints with exponent  $b = 1.14 \pm 0.05$ . (e) Comparison of  $n_c/N$  across the melting transition for different  $p$  values. The points along x-axis are shifted by their corresponding  $q_m$  values to coincide with zero. All data shown for length  $N = 500$  and averages are taken according to Eq. (5).

is fixed across melting, naturally  $T_m$  where the chains get separated increases (equivalently  $q_m$  decreases). Noticeably, the effect of lattice heterogeneity gets prominent for larger system sizes and  $p \lesssim 0.6$ , e.g., as reflected in the divergence of the specific heat [Fig. 2(d)].

Fitting the melting points for  $p > p_c$  with a straight line of the form  $y = mx + c$ , we get the slope  $m = 3.78196 \pm 0.01048$  and the y-intercept to be  $c = 0.0354181 \pm 0.006505$ . Extrapolating this fitted line, we obtain the melting point at the percolation threshold to be  $q_m(p_c) = 1.215 \pm 0.01$ . Additionally, from simulations performed at  $p = 0.312$ , the melting point is  $q_m = 1.21 \pm 0.05$  [Fig. 2(e)]. The melting points  $q_m(p_c)$  thus obtained using two different methods lie well within each other’s error bounds.

For values of  $p \lesssim 0.4$ , with growing sample-to-sample fluctuation, the convergence of the higher moments of the order parameter (such as  $n_c^2$ ) and, therefore, the cumu-

lants (such as  $C_c$ ) calculated from it, is difficult, which led us to estimate  $q_m$  relying only upon the first moment, i.e.,  $n_c$  itself. We found Eq. (5) and Eq. (6) gives nearly identical values for  $n_c$ , with Eq. (6) giving slightly larger  $q_m$ ’s for  $p \neq 1$  and same for  $p = 1$ . Similar equivalence for single polymers in disordered media was pointed out in the past [4, 9, 48], and more recently for semi-stiff polymers in heterogeneous lattices using flatPERM [6]. Interestingly, we observe a faster convergence when using Eq. (6) with the same  $\eta_2$ .

*A sharper transition:* Besides increasing  $T_m$ , the transition also gets sharper as  $p \rightarrow p_c$ . As evidence, we plot the energy density ( $n_c/N$ ) calculated using Eq. (5), across a wide range of temperatures on both sides of the melting point for different  $p$  values up to the percolation critical point [see Fig. 2(e)]. The points along the x-axis are shifted by their corresponding melting temperatures, i.e.,  $q - q_m$ . Noticeably, the jump in  $n_c$  around  $q_m$  grows

sharper as  $p$  is decreased when data of the same system size (here  $N = 500$ ) is compared. The conclusion remains invariant even when Eq. (6) was used for averaging. If there is a change in the exponent  $\phi$ , albeit slightly, is hard to confirm because of large sample fluctuations leading to poor convergence even after running the program for weeks.

A similar argument as before can explain the increase in the sharpness; upon decreasing  $p$ , it becomes increasingly difficult for the two strands to reunite (and form a bubble) due to the lack of available sites. Therefore, a situation arises for a sufficiently disordered medium where the in-between states connecting the bound and unbound phases are suppressed. This results in an abrupt unbinding of the strands, as observed from Fig. 2(e). To verify this description, we look at the distribution of  $n_c$  in the upcoming paragraph.

*Order parameter distribution:* The order parameter per se is not enough to reveal all the crucial details of the melting transition and, therefore, we need to look at its distribution  $P_{n_c}(q)$  as well, especially, close to the transition point. In Fig. 3(a), we plot  $P_{n_c}$  near the melting point for  $p = 0.5$ , comparing data for chain lengths  $N = 100 - 500$ . Here, we take an extra averaging over 10 independent runs. Clearly, even at this small system size, one can easily distinguish the growing peak at  $n_c/N \sim 0.6$  and a deepening valley for the intermediate  $n_c$  values, which is absent for  $p = 1$  even at long lengths [8]. The absence of any peak for  $N = 100$  denotes that the effect of lattice heterogeneity has not been felt by the DNA strands yet to the extent that it modifies the distribution, but that changes for longer chain lengths at  $N = 500$ . This further suggests that not all parts of the DNA experience the same environment (entropy), and melting happens heterogeneously along the chain with the bulk melting temperature given by an averaged value over the chain. Next, in Fig. 3(b), we plot the scaling form of  $P_{n_c}(q_m)$  for different  $p$  values and fixed system size of  $N = 500$ . Notice how the right peak representing the bound phase becomes more prominent while approaching  $n_c/N = 1$  and a further deepened valley for  $p = 0.5$  at  $n_c/N \approx 0.3$ .

To understand the above behavior, note that a first-order transition is generally characterized by a doubly peaked distribution separated by a valley whose depth grows with the system size as  $\exp(-\sigma L^{d-1})$ . The valley results from the  $d - 1$  dimensional surface separating the coexisting phases in the  $d$ -dimensional Euclidean space embedding the system. For our model DNA, which is topologically one-dimensional, any valley separating the bound and unbound states is absent for  $p = 1$  since, while going from a bound segment to an unbound segment along the DNA chain, there is no surface energy-like cost that is extensive and, therefore, the states in-between are not suppressed. On the other hand, for DNA in a sufficiently disordered environment, the emerging valley results from the ensuing entropy crisis, suppressing the intermediate states thereof. For  $n_c/N \rightarrow 0$ , config-

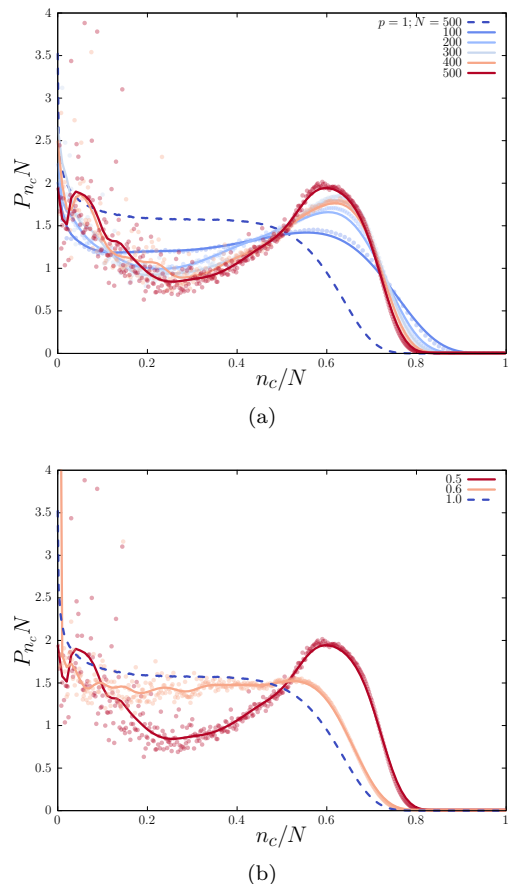


FIG. 3. **Order parameter distribution.** (a) Scaling of order parameter distribution with system size at the melting point of  $p = 0.5$  around  $q_m = 1.93$ . Data shown corresponds to lengths  $N = 100 - 500$ . For comparison, we have also shown data for  $p = 1$  at  $q_m = 3.825$  for  $N = 500$  as dashed line. Solid lines are approximation of the data with Bézier curve. (b) Comparison of scaled order parameter distribution for  $p = 1, 0.6$  and  $0.5$  for system size  $N = 500$ .

urations of two individual strands of effective length  $2N$  need to be sampled, resulting in an increased fluctuation of the  $P_{n_c}$  curve as compared to the  $n_c/N > 0.6$  side.

*Reunion or bubble statistics:* Next, we come to bubble statistics, where we find the bubble-size-distribution ( $P(\ell_b)$ ) at the corresponding transition points, the average number of bubbles per unit length ( $n_b$ ), and the average bubble length ( $\langle \ell_b \rangle$ ) for different  $p$  values. At the melting point, the bubble-size-distribution (BSD) follows a power law of the form  $P(\ell_b) \sim \ell_b^{-c}$ , where  $c$  is the reunion exponent [7]. The advantage of measuring  $c$  is that it is robust with system size and, therefore, less affected by finite size corrections. The exponent  $c$  connects to the exponent  $\phi$  as  $\phi = c - 1$  for continuous transitions and is also a measure for the sharpness of the transition.

In Fig. 4, we plot the BSD at their corresponding melting points for  $p = 1$  to  $0.312$ . The exponent  $c$  is extracted by fitting the intermediate data points

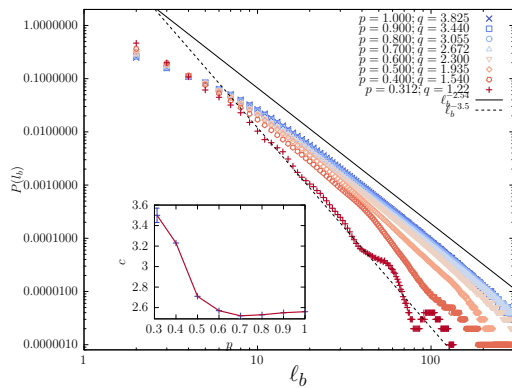


FIG. 4. **Bubble size distribution.** Bubble size distribution at the melting points of  $p$  from 1 – 0.312. The straight line is a fit of the  $p = 1$  data points in the range  $\ell_b = 20 - 100$  giving  $c = 2.54$  [29], and the dotted line for the data points of  $p = 0.312$  in the same range giving  $c = 3.5$ . (Inset) The variation of the exponent  $c$  for different values of  $p$ .

in the range  $\ell_b = 20 - 100$ , which comes out to be  $c = 2.54 \pm 0.005$  [29] for  $p = 1$  and  $c = 3.5 \pm 0.06$  for  $p = 0.312$ . A similar increase in the exponent for loop formation was found for polymer in correlated disorder in Ref. [22]. In the inset of Fig. 4, we show the variation of the exponent  $c$  with  $p$ . Noticeably, the major observable change in the value of  $c$  happens mainly for  $p \lesssim 0.6$ , while it remains almost the same above  $p = 0.6$ , akin to what we found for the scaling of  $C_c$  peaks in Fig. 2(d). On this basis, we categorize the effect of disorder on DNA melting into two distinct regimes: the weak disorder regime for  $p \in [0.6, 1]$ , and the strong disorder regime for  $p \in [0.312, 0.6)$ . The increase in the value of  $c$  is another evidence for the sharpening of the melting transition. The BSD for  $p = 0.4$  and 0.312 shows undulant behavior at longer bubble sizes, which is absent for higher  $p$  values. This behavior is because for  $p$  close to  $p_c$ , entropically rich regions within an infinite cluster are often connected by entropically unfavorable regions (bottlenecks) which forces the two strands to reunite and form a bubble at specific lengths, giving rise to intermittent rise in  $P(\ell_b)$  value.

The two main length scales in the DNA melting problem come from the separation of the DNA strand end-points in space ( $\zeta_1$ ) and the other from the mean diameter of the melted bubbles ( $\zeta_2$ ), which is approximately connected to what we find as  $\ell_b$ . These two length scales are controlled by two critical exponents, which we call  $\nu_1$  and  $\nu_2$ . The exponent  $\nu_2$  controls how the length scale  $\zeta_2 \sim |q - q_m|^{-\nu_2}$  diverges at the melting point. It was previously discussed how we can write  $\phi = \nu_1/\nu_2$  [8] using these two exponents. For the pure melting problem, these two exponents are the same  $\nu_1 = \nu_2$  and therefore  $\phi = 1$ . With a disordered background, we expect a change in how these length scales diverge.

We found that the average bubble length ( $\ell_b$ ) decreases in the disordered environment to the extent that for  $p \rightarrow$

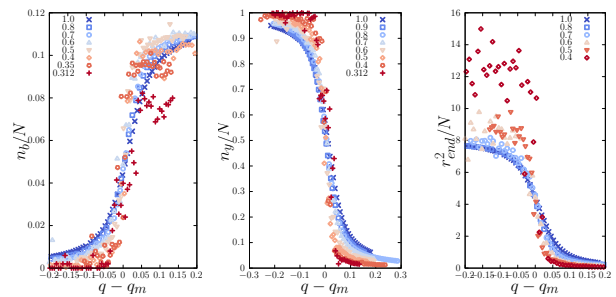


FIG. 5. **Bubble number and Y-fork.** Comparison of (a) average number of bubbles, (b) fraction of broken bonds in the y-fork, and (c) difference of the end points of the two strands squared, for different values of  $p$  across melting transition. To compare we shift the x-axis by the corresponding melting points  $q_m$ 's of each  $p$ .

$p_c$  near the melting transition from the bound side ( $\langle \ell_b \rangle \approx 2$ ), which means at  $q \approx q_m^+$  the DNA is punctured with many bubbles of the smallest possible size. The increase in the number of bubbles ( $n_b$ ) for  $q \rightarrow q_m^+$  remains sharp for smaller  $p$ 's, a la number of base pair contacts ( $n_c$ ). However, towards the bound side close to the melting point for  $p \gtrsim 0.4$ , we found  $n_b$  to reduce compared to  $0.4 < p < 1$  [Fig. 5(a)]. Similar effects, corroborating a sharper transition, are also seen for the number of broken bonds in the Y-fork per unit length ( $n_y/N$ ) towards the wandering end [Fig. 5(b)] and the separation in the chain end points squared ( $r_{end}^2$ ) [Fig. 5(c)] for  $p < 1$ .

Finally, to show that our simulations are not glitched by incomplete sampling where few configurations contribute largely to the statistics, we show the contributions of each sample to the partition sum by comparing the distribution of four weights  $P(\ln W)$ , and its weighted distribution  $WP(\ln W)$  [18] for  $p = 0.8$  at  $q_m = 3.055$  in Fig. 6. Note that  $WP(\ln W)$ 's contribution is large where  $P(\ln W)$  is appreciable.

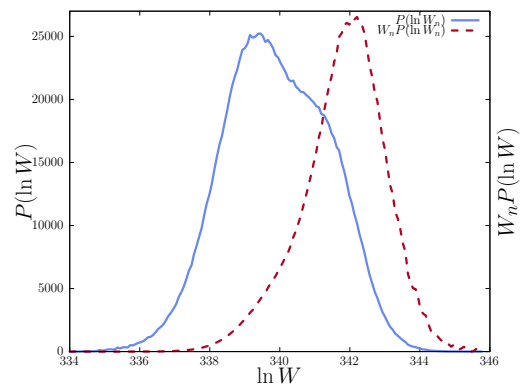


FIG. 6. **Sampling statistics.** Four weight distribution  $P(\ln W)$  and its rescaled weighted distribution  $WP(\ln W)$  at  $q_m = 3.055$  for  $p = 0.8$ . The weight  $W$  is exact up to a multiplicative constant ( $\ll 1$ ) to contain numerical overflow.

## VI. CONCLUSION

In conclusion, we studied the effect of disordered media on the melting of a lattice DNA model. Our findings clearly demonstrate that besides stabilizing the bound ds phase against thermal fluctuations, the presence of atmospheric disorder also increases the cooperativity (sharpness) of the melting transition. Melting, therefore, remains a first-order transition with no substantial change in the scaling exponent characterizing the melting transition. These findings suggest that media disorder can be considered relevant for DNA denaturation in the renormalization group sense, although it does not change the universality class.

The most dramatic effect is perhaps the change in the probability distribution of the number of base-pair contacts near the melting point, which reveals that, for a sufficiently disordered environment, during the transition, the states in between the bound and unbound phases are suppressed, thereby revealing a stronger first-order nature of the melting transition as observed from the emerging double peaks in the distribution. Evidence for a sharper transition is also present from other observables, such as the order parameter and how its fluctuation scales with the system size at the melting point, the bubble size distribution, etc., to support our conclusions. Quenched and annealed averaging of the order parameter did not show any substantial difference.

Coming to the question of whether there is a melting transition at the percolation critical point, we used two different methods to identify the melting temper-

ature at  $p_c$ ; first, extrapolating the estimated melting temperatures obtained at lower values of disorder, where the melting temperatures were calculated with a higher accuracy, and secondly, by simulating sufficiently close to the critical point. These two estimates are well within each other's error. As a caution, estimating the melting points becomes increasingly difficult with decreasing  $p$  ( $\lesssim 0.4$ ), and convergence of the order parameter cumulants is difficult due to the inherent enhanced sample-to-sample fluctuations. Therefore, one can only rely upon the first moment – the order parameter itself – to find the melting points.

Lastly, while disorder comes in many different forms, we consider the simplest possible case of repulsive non-correlated type for our study. Depending upon the electrostatic interaction, the disorder can be attractive too, with long-range correlations [21]. Such considerations are currently underway, which we aim to publish in the future.

## VII. ACKNOWLEDGEMENT

DM would like to thank Deepak Dhar, Somendra M Bhattacharjee, and Soheli Mukherjee for insightful discussions and valuable feedback during the research work. DM was supported by the BCSC Fellowship from the Jacob Blaustein Center for Scientific Cooperation and by the Israel Science Foundation (ISF) through Grant No. 1301/17 and 1204/23.

- 
- [1] Atmosphere refers to the immediate environment of the DNA.
  - [2] M Bachmann and W Janke. Thermodynamics of lattice heteropolymers. *J. Chem. Phys.*, 120(14), 2004.
  - [3] H. G. Ballesteros and et al. Critical exponents of the three-dimensional diluted ising model. *Phys. Rev. B*, 58(5):27402747, 1998.
  - [4] V Blavatska. Equivalence of quenched and annealed averaging in models of disordered polymers. *J. of Phys. Cond. Matt.*, 25(505101), 2013.
  - [5] V Blavatska and W Janke. Shape anisotropy of polymers in disordered environment. *J. Chem. Phys.*, 133(184903), 2010.
  - [6] C J Bradly and A L Owczarek. Effect of lattice inhomogeneity on collapsed phases of semi-stiff isaw polymers. *J. Stat. Phys.*, 182(27), 2021.
  - [7] E Carlon, E Orlandini, and A L Stella. Roles of stiffness and excluded volume in dna denaturation. *Phys. Rev. Letts.*, 88(19), 2002.
  - [8] M. S. Causo, B. Coluzzi, and P. Grassberger. Simple model for the dna denaturation transition. *Phys. Rev. E*, 62(3), 2000.
  - [9] B J Cherayil. Equilibrium dimensions of polymers in quenched disorder. *J. Chem. Phys.*, 92(6246), 1990.
  - [10] P Dey and A Bhattacharjee. Role of macromolecular crowding on the intracellular diffusion of dna binding proteins. *Scientific Reports*, 8(844), 2018.
  - [11] P. Le Doussal and J Machta. Self-avoiding walks in quenched random environments. *J. Stat. Phys.*, 64(3/4), 1991.
  - [12] Titus S. van Erp and et. al. Can one predict dna transcription start sites by studying bubbles? *Phys. Rev. Letts.*, 95(218104), 2005.
  - [13] H Frauenkron, M. S. Causo, and P Grassberger. Two-dimensional self-avoiding walks on a cylinder. *Phys. Rev. E*, 59(1), 1999.
  - [14] Alice B Fulton. How crowded is the cytoplasm? *Cell*, 30:345–347, 1982.
  - [15] S Geggier and A Vologodskii. Sequence dependence of dna bending rigidity. *Proc. Natl. Acad. Sci. USA*, 107(15421), 2010.
  - [16] S Ghosh and et al. Nearest-neighbor parameters for predicting dna duplex stability in diverse molecular crowding conditions. *PNAS*, 117(25), 2019.
  - [17] P. Grassberger. Pruned-enriched rosenbluth method: Simulations of  $\theta$  polymers of chain length up to 1 000 000. *Phys. Rev. E*, 56(3), 1997.
  - [18] P Grassberger. Comment on “polymer localization in attractive random media”. *J. Chem. Phys.*, 111:440–442,



- 1999.
- [19] A. B. Harris. Effect of random defects on the critical behaviour of ising models. *J. Phys. C: Solid State Physics*, 7(1671), 1974.
- [20] K. S Harve and et al. Understanding how the crowded interior of cells stabilizes dna/dna and dna/rna hybrids—in silico predictions and in vitro evidence. *Nucl. Acids. Res.*, 38(1), 2010.
- [21] K Haydukivska and V Blavatska. Ring polymers in crowded environment: Conformational properties. *J. Chem. Phys.*, 141(094906), 2014.
- [22] K Haydukivska and V Blavatska. Loop statistics in polymers in crowded environment. *J. Chem. Phys.*, 144(084901), 2016.
- [23] F Hong, J. S. Schreck, and P Šulc. Understanding dna interactions in crowded environments with a coarse-grained model. *Nucl. Acids. Res.*, 48(19), 2020.
- [24] Y. L. Kermanpour, H. L. Liu, Y. Hu, Y. Z. Shang, S. I. Sandler, and J. W. Jiang. Molecular thermodynamic model for dna melting in ionic and crowded solutions. *J. Phys. Chem. B*, 114(9905-9911), 2010.
- [25] S B Lee and H Nakanishi. Self-avoiding walks on randomly diluted lattices. *Phys. Rev. Letts.*, 61(18), 1988.
- [26] D Majumdar. Elasticity of a dna chain dotted with bubbles under force. *Phys. Rev. E*, 103(052412), 2021.
- [27] D Majumdar. Adsorption of melting deoxyribonucleic acid. *Phys. of Fluids*, 35(067110), 2023.
- [28] D Majumdar. Dna melting in poor solvent. *J. Stat. Phys.*, 190(14), 2023.
- [29] D Majumdar and S. M. Bhattacharjee. Softening of dna near melting as disappearance of an emergent property. *Phys. Rev. E*, 102(032407), 2020.
- [30] D Majumdar, S Singh, and R Granek. (in preparation).
- [31] Neha Mathur, Amar Singh, and Navin Singh. Force-induced unzipping of dna in the presence of solvent molecules. *Biophysical Chemistry*, 307(107175), 2024.
- [32] Y Meir and A. B. Harris. Self-avoiding walks on diluted networks. *Phys. Rev. Letts.*, 63(26), 1989.
- [33] K Metze. Fractal dimension of chromatin: potential molecular diagnostic applications for cancer prognosis. *Expert Review of Molecular Diagnostics*, 13(7):719–735, 2013.
- [34] Daisuke Miyoshi and Naoki Sugimoto. Molecular crowding effects on structure and stability of dna. *Biochimie*, 90:1040–1051, 2008.
- [35] S Nakano and et al. The effect of molecular crowding with nucleotide length and cosolute structure on dna duplex stability. *J. AM. CHEM. SOC.*, 126(14330-14331), 2004.
- [36] D Poland and H. A. Scheraga. Phase transitions in one dimension and the helix—coil transition in polyamino acids. *J. Chem. Phys.*, 45:1456–1463, 1966.
- [37] M. D. Rintoul, Jangnyeol Moon, and Hisao Nakanishi. Statistics of self-avoiding walks on randomly diluted lattices. *Phys. Rev. E*, 49(4), 1994.
- [38] J.-L Sikorav and G M Church. *J. Mol. Biol.*, 222:1085–1108, 1991.
- [39] A Singh and N Singh. Dna melting in the presence of molecular crowders. *Phys. Chem. Chem. Phys.*, 19(19452), 2017.
- [40] A R Singh, D Giri, and S Kumar. Effects of molecular crowding on stretching of polymers in poor solvent. *Phys. Rev. E*, 79(051801), 2009.
- [41] Amar Singh, Arghya Maity, and Navin Singh. Structure and dynamics of dsdna in cell-like environments. *Entropy*, 24(1587), 2022.
- [42] S Singh and R Granek. Active fractal networks with stochastic force monopoles and force dipoles unravel subdiffusion of chromosomal loci. *arXiv:2307.12310v2*, 2024.
- [43] Tomasz Skóra, Farzaneh Vaghefikia, Jörg Fitter, and Svyatoslav Kondrat. Macromolecular crowding: How shape and interactions affect diffusion. *J. of Phys. Chem. B*, 124:7537–7543, 2020.
- [44] Dietrich Stauffer. *Introduction to percolation theory*. Taylor & Francis, London, 2nd edition.
- [45] M V Tamm, L I Nazarov, A A Gavrilov, and A V Chertovich. Anomalous diffusion in fractal globules. *Phys. Rev. Lett.*, 114(178102), 2015.
- [46] Stephanie C Weber, Andrew J Spakowitz, and Julie A Theriot. Nonthermal atp-dependent fluctuations contribute to the in vivo motion of chromosomal loci. *PNAS*, 109(19):7338–7343, 2011.
- [47] R Wieder and J. G. Wetmur. *Biopolymers*, 20:1537–1547, 1981.
- [48] D Wu, K Hui, and D Chandler. Monte carlo study of polymers in equilibrium with random obstacles. *J. Chem. Phys.*, 96(835), 1991.
- [49] C Yuan, E Rhoades, X W Lou, and L A Archer. Spontaneous sharp bending of dna: Role of melting bubbles. *Nucl. Acids. Res.*, 34(4554), 2006.
- [50] S B Zimmerman. Macromolecular crowding effects on macromolecular interactions: some implications for genome structure and function. *Biochimica et Biophysica Acta*, 1216:175–185, 1993.